

Liquid Front Profiles Affected by Entanglement-induced Slippage

O. Baumchen, R. Fetzner, and K. Jacobs[†]

Department of Experimental Physics, Saarland University, D-66041 Saarbrücken, Germany.

(dated: February 22, 2024)

Hydrodynamic slippage plays a crucial role in the flow dynamics of thin polymer films, as recently shown by the analysis of the profiles of liquid fronts. For long-chained polymer films it was reported that a deviation from a symmetric profile is a result of viscoelastic effects. In this Letter, however, evidence is given that merely a slip boundary condition at the solid/liquid interface can lead to an asymmetric profile. Dewetting experiments of entangled polymer melts on diverse substrates allow a direct comparison of rim morphologies. Variation of molecular weight M_w clearly reveals that slippage increases dramatically above a certain M_w and governs the shape of the rim. The results are in accordance with the theoretical description by de Gennes.

PACS numbers: 68.15.+e, 83.50.Lh, 83.80.Sg, 47.61.-k

The controlled manipulation of small liquid volumes is one of the main tasks in the field of micro- and nanofluidics. In this context, the role of hydrodynamic slippage has attracted much attention due to its enormous relevance for applications such as lab-on-chip devices. A variety of experimental methods exist to characterize slippage. The large number of techniques and results is summarized and discussed in recent review articles [1, 2, 3].

If a thin liquid film on top of a solid substrate can gain energy by minimizing its interfacial area, the film ruptures and holes occur (see [4], [5] and references therein). These dry circular patches grow with time, and the removed liquid accumulates in a rim surrounding the holes along their perimeter. Dewetting of thin liquid films on solid substrates is a result of internal capillary forces, which can be inferred from the effective interface potential [6, 7]. Viscous dissipation within the liquid, which mainly occurs at the three-phase contact line [8], and friction at the solid/liquid interface (slippage) counteract these driving forces. Concerning the characteristic dynamics of hole growth (hole radius R versus time t), Brochard-Wyart and colleagues [8] proposed a sequence of different stages starting with the birth of a hole, which is characterized by an exponential increase of the dewetting velocity (denoted by $V = dR/dt$). It is followed by a regime that is governed by the formation of the rim and dominated by viscous flow ($R \propto t$), followed by a stage of a "mature" rim, where surface tension rounds the rim and slippage might be involved. In case of full slippage, a growth law $R \propto t^{2/3}$ is expected. This view was supplemented by an experimental study by Dammann and colleagues, who associated different dewetting regimes with corresponding rim shapes in case of viscoelastic fluids [9]. Vilim in et al. presented a theoretical approach taking viscoelastic properties and slippage into account [10]. In our earlier studies, we experimentally examined rim profiles of dewetting long-chained PS films on hydrophobized Si wafers and attributed the transition from symmetric ("oscillatory") to increasingly asymmetric ("monotonically decaying") shapes with the molecular weight of the polymer to viscoelastic effects [11]. These results go along with a phenomenological model that predicts a phase diagram for rim morphologies [12].

These previous studies, however, lack one facet, which by now has been identified as one of the major issues in unifying dewetting dynamics and profiles: hydrodynamic slippage. In our recent studies we focused our interest on slippage of polymer melts, where polymers were used exclusively below their entanglement length [13, 14, 15]. In this Letter, the studies are extended to long-chain polymer melts. Our aim is to characterize slippage of polystyrene films above their entanglement length. This might involve new problems related to non-Newtonian behavior due to viscoelastic flow and stress relaxation. The latter has been reported to cause polymer thin film rupture [16, 17] and to impact the early stage of dewetting [17]. As will be shown in the following for the mature stage, residual stress and viscoelastic properties have no impact on the shape of dewetting rims, if low shear rates are involved. It will be demonstrated that in that stage, asymmetric rim profiles are caused by slippage only.

Films of atactic polystyrene (PSS Mainz, Germany) with molecular weights ranging from 5.61 to 390 kg/mol (termed e.g. PS (390k)) and low polydispersity ($M_w/M_n = 1.02 - 1.09$) were spin-cast from toluene solutions on freshly cleaved mica sheets and transferred to smooth hydrophobized Si wafers with a native oxide layer (obtained from Siltronic, Burghausen, Germany) by coating them on a MilliporeTM water surface. To avoid residual stresses in films above the entanglement length of PS, the films were pre-annealed on the mica substrate well above their glass transition temperature (up to 3 hours at 140 °C) [16]. The prepared film thicknesses h_0 varied between 100 and 140 nm. Hydrophobization was either achieved through standard silanization techniques [18] using self-assembled monolayers of octadecyltrichlorosilane (OTS) and dodecyltrichlorosilane (DTS)

[†] Present address: Ian Wark Research Institute, University of South Australia, Mawson Lakes, SA 5095, Australia.

[†] Electronic address: k.jacobs@physik.uni-saarland.de

TABLE I: Substrate properties.

layer	d (nm)	rms (nm)	adv (°)	(°)	sv (mN/m)
AF 1600	21 (1)	0.30 (3)	128 (2)	10	15.0
OTS	2.3 (2)	0.09 (1)	116 (1)	6	23.9
DTS	1.5 (2)	0.13 (2)	114 (1)	5	26.4

or by preparing a thin amorphous te on layer (AF 1600) using the spin-coating technique. The thickness d and the root-mean-square (rms) roughness of the hydrophobic layers (see Tab. I) were measured via ellipsometry (EP³, Nano Inn, Göttingen, Germany) and atomic force microscopy (AFM, Multimode, Veeco Instruments, Santa Barbara, CA, USA). Additionally, substrates are characterized in terms of their wetting properties by their contact angles (advancing α_{adv} , and contact angle hysteresis α_h) of MilliporeTM water and their surface energy γ_{sv} (via measuring the contact angles of apolar liquids).

Nucleation and subsequent growth of holes starts after heating the samples above the glass transition temperature of the PS melt. In the following, optical microscopy is utilized to dynamically monitor the size of growing holes. At a certain hole radius (about 12 μ m) in the mature regime, the experiment is stopped by quenching the sample to room temperature. The profile of the rim is then imaged by AFM [19]. As shown in Fig. 1 a), comparing rim profiles for the same molecular weight, film thickness and viscosity (for the respective dewetting temperature) clearly exhibits strong differences that can exclusively be ascribed to the different substrates. For e.g. PS (65k) at 130 °C an oscillatory profile with a "trough" on the "wet" side of the rim is observed on the AF 1600 substrate. A close-up of the trough is given in the inset. Yet, in the case of OTS and DTS, rims are found that decay monotonically into the unperturbed polymer film.

In Fig. 1 b), experimental profiles are shown for the AF 1600 substrate, where the molecular weight of the polymer melt is varied. In case of PS (65k), we observe a clearly oscillatory profile, whereas for e.g. PS (186k) or higher molecular weights, asymmetric (monotonically decaying) rim morphologies are recorded. Hence, an increase in M_w on the identical substrate provokes the same morphological differences in rim shapes as before (Fig. 1 a)) the variation of the substrate. To probe whether or not the effect is merely a result of the melt viscosity, the dewetting temperature on AF 1600 (see Tab. II) was additionally varied. Yet, no systematic influence of the viscosity on the rim profiles is found for this substrate, as exemplarily shown for PS (186k) in the inset of Fig. 1 b). The observed marginal differences of the rim profiles can be related to small variations of accumulated material (via slightly different hole radii and film thickness in different experiments).

Summarizing the qualitative observations, we find that an increase in molecular weight strongly amplifies the asymmetry of the profiles in the same manner as a change of substrate is capable of causing. According to

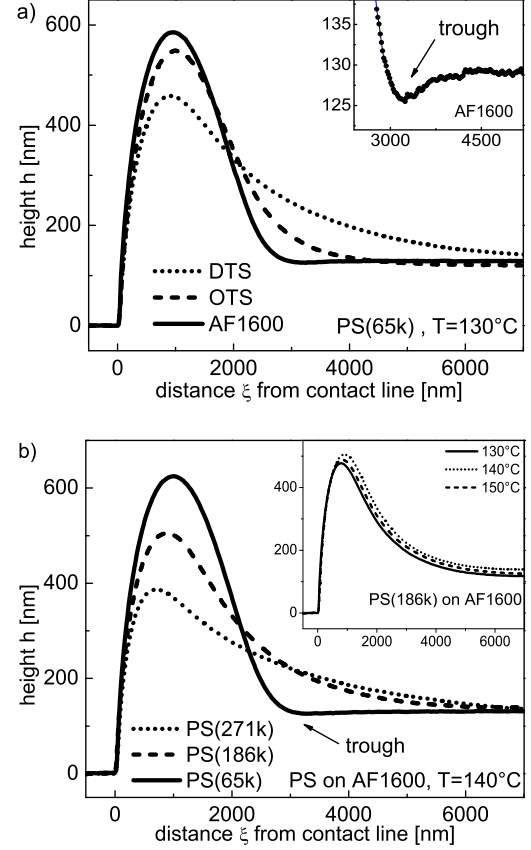


FIG. 1: a) Rim profiles of PS (65k) on DTS (dotted), OTS (dashed) and AF 1600 (solid line) at 130 °C. The inset illustrates the oscillatory behavior on AF 1600. b) Rim shapes on AF 1600 for different molecular weights (140 °C, PS (65k), PS (186k), PS (271k)). Inset: Variation of viscosity via different temperatures for the same molecular weight (see Tab. II) shows insignificant influence on rim profiles.

our previous studies on OTS and DTS concerning non-entangled PS melts, asymmetric rims are related to slippage [13, 14, 15]. For DTS, slip lengths b of up to 5 μ m were obtained, for OTS, values are about one order of magnitude smaller. The question now arises as to the manner in which slippage correlates to the molecular weight and the number of entanglements in the AF 1600 system. To quantify slippage there, rim profiles will be analyzed.

As shown recently, lubrication models for Newtonian flow and different slip conditions (no-slip, weak-slip, intermediate-slip and strong-slip [20]) and a more generalized model based on the full Stokes equations [14] can be applied to thin dewetting films with the important result that values for the slip length b can be obtained.

To assess whether these models might be used to analyze the experimental data, the impact of viscoelasticity on fluid flow needs to be estimated: The Weissenberg number $Wi = \tau \dot{\gamma}$ relates the time scale of stress

TABLE II: Comparison of viscosities (obtained from the WLF equation), calculated relaxation times and measured rim widths w (on AF 1600) given for a selection (see Fig. 1) of dewetting temperatures T and molecular weights M_w .

M_w	T (°C)	(Pa s)	(s)	w (μm)
65k	130	$1.3 \cdot 10^6$	6.5	2.73
65k	140	$1.6 \cdot 10^5$	0.8	2.81
186k	130	$4.4 \cdot 10^7$	222	5.02
186k	140	$5.6 \cdot 10^6$	28.1	4.86
186k	150	$1.1 \cdot 10^6$	5.4	5.29
271k	140	$2.0 \cdot 10^7$	100.5	7.47

relaxation with the time scale of applied shear γ . Relaxation times are determined from the corresponding viscosities and the shear modulus $G = 0.2 \text{ MPa}$ (for PS, [21]) via $\tau = \eta/G$ (see Tab. II). Evaluation of the shear rates within the moving rim is based on $\dot{\gamma} = \max(|\partial_x u_x|; |\partial_z u_x|) = \max(|\dot{\gamma}_x|; |\dot{\gamma}_z|)$, where $\dot{\gamma}$ is the dewetting speed (identified as the dominant velocity $u_x = u_z$ within the rim) which can be inferred from optical hole radius measurements. The lateral displacement x is estimated as the width w of the rim. The value w is defined as the distance between the three-phase contact line and the position where the rim height has dropped to 110% of the film thickness h_0 , i.e. $h(w) = 1.1h_0$. The vertical displacement z is given by $z = h_0 + b$, where b denotes the slip length as determined by the quantitative rim analysis described in the last part of this Letter. The described estimation leads to values for Wi between 0.01 and 0.1 (on AF 1600) and 0.5 (on OTS/DTS). An influence of viscoelastic effects on flow dynamics is expected for Weissenberg numbers of 1 and larger. In that case, a model including viscoelasticity has to be used [22]. Low shear rates as described above and the pre-annealing step after spin-coating allow us to safely exclude viscoelastic effects as the source of different rim morphologies. This consideration justifies the assumption of Newtonian flow, on which the following data analysis is based.

The theoretical description of the model for Newtonian liquids presented in [14] is derived from the full Stokes equations in two dimensions for a viscous, incompressible liquid including the Navier slip-boundary condition $b = u = \partial_z u|_{z=0}$, where u denotes the velocity in x -direction and z the vertical scale. This leads to the equations of motion for a flat liquid film. Then, a linear stability analysis is applied by introducing a small perturbation $h = h_0 + \delta h(x; t)$ and velocity $u(x; t)$ to the undisturbed state $h = h_0$ and $u = 0$. In the co-moving frame $\xi = x - s(t)$, where $s(t)$ is the position of the rim, a quasi-stationary profile evolves. Solving the linear equation using the normal modes ansatz $h = h_0 \exp(k\xi)$ and $u = u_0 \exp(k\xi)$ gives a characteristic equation for k which is expanded up to third order according to the Taylor formalism:

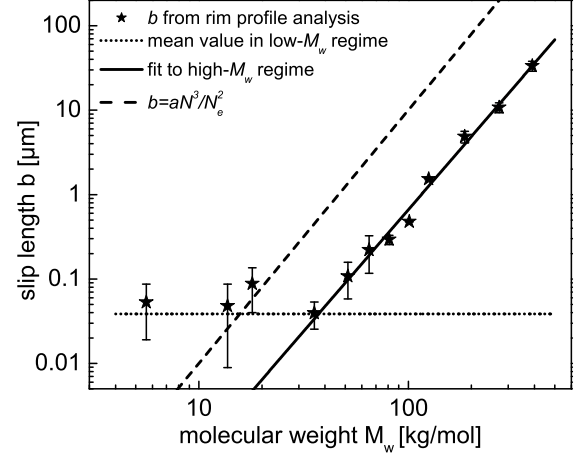


FIG. 2: Slip lengths of PS films on AF 1600 obtained from rim profile analysis. Each data point represents the average value of different measurements (2–3 measurements for each M_w value above 35.6k and 5 or more below). The solid line represents a fit to the experimental data from PS (35.6k) to PS (390k), the dashed line visualizes $b = aN_e^3/N_e^2$ using values for a and N_e given in the literature [21]. The dotted line represents the average of slip lengths for melts from PS (5.61k) to PS (18k).

$$\left(1 + \frac{h_0}{3b}\right)(h_0 k)^3 + 4Ca \left(1 + \frac{h_0}{2b}\right)(h_0 k)^2 - Ca \frac{h_0}{b} = 0; \quad (1)$$

where Ca denotes the capillary number given by $Ca = \dot{\gamma} b / \sigma$. Hence, rim profiles depend on the capillary number Ca and the ratio of slip length b to film thickness h_0 . Eq. (1) implies that a morphological transition from oscillatory (complex conjugate solutions for k) to monotonic (real k values) decaying rim shapes occurs if $Ca^2 > (3^3(b=h_0+1=3)^2) = (4^4(b=h_0+1=2)^3)$ on slippery substrates (large $b=h_0$) and for large capillary numbers Ca [14, 15]. Furthermore, Eq. (1) predicts progressively asymmetric rims for increasing values of $b=h_0$.

In the following, PS melts on the AF 1600 substrate are considered: Rim profiles are evaluated by fitting the wet side of the rim with a damped oscillation (oscillatory profiles, up to PS (81k)) or a simple exponential decay (monotonic rims, for PS (101k) and above).

In the case of an exponential decay, a single value for k is gained from the experimental data. Knowing the film thickness h_0 and the capillary number Ca (from independent rim velocity data), this k value allows us to calculate the respective slip length via Eq. (1). For oscillatory profiles, k is a pair of complex conjugate numbers. From these two independent solutions, both the capillary number and the slip length can be extracted via Eq. (1) at the same time. Viscosity data calculated from these Ca values showed excellent agreement with theoretical values (from the WLF equation) and demonstrate

the consistency of the applied model. For further details concerning the fitting procedure and data evaluation, one should refer to previous publications [13, 14, 15].

The slip lengths b of a set of experiments, i.e. different dewetting temperatures and viscosities, are shown in Fig. 2 as a function of molecular weight M_w of the PS melt. Two distinct regimes can clearly be seen: Constant slip lengths in the order of 10 to 100 nm at small M_w and slip lengths that increase with the power of 2.9 (2) in case of larger M_w . The transition between both regimes occurs at 37 kg/mol, which is consistent with the critical value M_c of entanglement effects ($M_c = 35$ kg/mol for PS according to [21]). For the same viscosity (e.g. $2 \cdot 10^6$ Pas) in case of e.g. PS (51.5k) and PS (271k), an enormous difference in slippage of two orders of magnitude solely due to the difference in chain length is obtained. We therefore state that slippage is directly related to entanglements rather than viscosity. Besides the fact that an influence of the melt viscosity (via temperature variation) for a certain molecular weight could not be detected, even experiments omitting the pre-annealing step after preparation on mica do not show significant impact. Additionally, we want to emphasize that careful analysis of the dewetting velocity data from hole growth dynamics (of the identical samples), according to the model presented in [23], confirmed the $b(M_w)$ behavior obtained from rim analysis [24].

For long polymer chains, described by the reptation model, de Gennes predicts a scaling of $b \propto N^{-3}$, where N denotes the number of monomers, which corroborates the experimental exponent of 2.9 (2) for experiments with $M_w > 35$ kg/mol as depicted in Fig. 2. According to the model, $b = aN^{-3} = N_e^2$, where N_e is the bulk entanglement length (number of monomers in an entanglement strand) and a a polymer specific molecular size, and is plotted in Fig. 2 as the dashed line for the literature values of

$N_e = 163$ [21] and $a = 3A$ [26] for PS. From the linear fit to our experimental data (solid line in Fig. 2), we obtain $a = N_e^2 = 1.12(7) \cdot 10^5 A$, which is one order of magnitude smaller than that expected by using the literature values given above. Keeping a from the literature, a significantly larger entanglement length of $N_e = 517$ results from the linear fit. This is an indication for a significantly lowered effective entanglement density in the vicinity of the substrate compared to the bulk and is in line with recent studies of thin polymer films [27, 28]. According to Brown and Russell, N_e of a polymer melt near an interface is expected to be about 4 times that in the bulk [29], which corroborates our experimental results.

To conclude, entanglements can strongly amplify slippage as deduced from dewetting experiments. Assigning asymmetric profiles exclusively to non-Newtonian effects such as viscoelasticity therefore turns out to be invalid. On the contrary, the hydrodynamic boundary condition, i.e. slippage, can dramatically provoke morphological changes in rim shape such as transitions from oscillatory to monotonic profiles. The onset of slippage correlates to the critical chain length for entanglements. The dependence of the slip length on molecular weight corroborates the description by de Gennes. To derive vice versa slip lengths solely from de Gennes' theory entails that bulk values for a and N_e (from literature) have to be used that might not appropriately describe polymer melts next to an interface. The method described here, however, represents a powerful tool to gain experimentally access to liquid flow properties at the solid/liquid interface and to quantify slip lengths.

We gratefully acknowledge financial support from German Science Foundation DFG under Grant Ja 905/3 within the priority program 1164 and generous support of Si wafers by Wacker Siltronic AG, Burghausen, Germany.

-
- [1] C. Neto et al., Rep. Prog. Phys. 68, 2859 (2005).
 - [2] E. Lauga et al., in Springer Handbook of Experimental Fluid Mechanics, edited by C. Tropea, A. L. Yarin, and J.F. Foss (Springer, Berlin Heidelberg New York, 2007).
 - [3] L. Bocquet and J.-L. Barrat, Soft Matter 3, 685 (2005).
 - [4] G. Reiter, Phys. Rev. Lett. 68 75 (1992).
 - [5] K. Jacobs, R. Seemann, and S. Herminghaus, in Polymer Thin Films, edited by O.K.C. Tsui and T.P. Russell (World Scientific, New Jersey London Singapore, 2008).
 - [6] A. Vrij, Discuss. Faraday Soc. 42 23 (1966).
 - [7] R. Seemann et al., Phys. Rev. Lett. 86, 5534 (2001).
 - [8] F. Brochard-Wyart et al., Langmuir 10, 1566 (1994).
 - [9] P. Dammann et al., Phys. Rev. Lett. 91, 216101 (2003).
 - [10] T. Vilim in et al., Europhys. Lett. 72, 781 (2005).
 - [11] R. Seemann et al., Phys. Rev. Lett. 87, 196101 (2001).
 - [12] S. Herminghaus et al., Phys. Rev. Lett. 89, 056101 (2002), Eur. Phys. J. E 12, 101 (2003).
 - [13] R. Fetzer et al., Phys. Rev. Lett. 95, 127801 (2005), Europhys. Lett. 75, 638 (2006).
 - [14] R. Fetzer et al., Langmuir 23, 10559 (2007).
 - [15] O. Baumchen et al., in IUTAM Symposium on Advances in Micro- and Nanofluidics, edited by M. Ellero, X. Hu, J. Frohlich, N. Adams (Springer, 2009).
 - [16] D. Podzimek et al. arXiv cond-mat/0105065v1 (2001).
 - [17] G. Reiter et al., Nature Materials 4, 754 (2005).
 - [18] S.R. Wassermann et al., Langmuir 5, 1074 (1989).
 - [19] Note that quenching the sample to room temperature has been proven not to change or influence the shape of the rim profile.
 - [20] A. Munch et al., J. Eng. Math. 53, 359 (2005).
 - [21] M. Rubinstein and R. Colby, Polymer Physics (Oxford University Press, 2003).
 - [22] R. Blobsey et al., Eur. Phys. J. E 20, 267 (2006).
 - [23] R. Fetzer and K. Jacobs, Langmuir 23, 11617 (2007).
 - [24] O. Baumchen and K. Jacobs, to be published.
 - [25] P.-G. de Gennes, C.R. Acad. Sci. B 288, 219 (1979).
 - [26] C. Redon et al., Macromolecules 27 468 (1994).
 - [27] L. Siet al., Phys. Rev. Lett. 94, 127801 (2005).
 - [28] D.R. Barbero and U. Steiner, Phys. Rev. Lett. 102, 248303 (2009).

- [29] H. R. Brown and T. P. Russell, *Macromolecules* 29 798 (1996).